

A MODEL FOR THE DIFFUSION OF FLUORESCENT PROBES IN THE SEPTATE GIANT AXON OF EARTHWORM

Axoplasmic Diffusion and Junctional Membrane Permeability

PETER R. BRINK* AND S. V. RAMANAN‡

**Department of Anatomical Sciences, Health Sciences Center, School of Medicine; and the*

‡*Department of Physics, State University of New York at Stony Brook, Stony Brook, New York 11794*

ABSTRACT The diffusion of the three fluorescent probes dichlorofluorescein, carboxyfluorescein, and Lucifer Yellow within the septate median giant axon of the earthworm was monitored using fluorometric methods. A diffusion model was derived that allowed computation of the apparent axoplasmic diffusion coefficient, junctional membrane permeability (septal membranes), and plasma membrane permeability for each probe. Dichlorofluorescein and carboxyfluorescein have similar apparent axoplasmic diffusion coefficients, which were reduced by a factor of eight relative to that predicted from the Einstein-Stokes equation. Nonspecific reversible binding appears to be the major cause of the retarded diffusion coefficients. Junctional membrane permeability for dichlorofluorescein was 4.7 to 73-fold greater than that for carboxyfluorescein. This difference could not be explained on the basis of molecular size but can be explained by the difference in charge between the two molecules. Diffusion coefficients and junctional membrane permeabilities remained constant with time for both dyes. The diffusion of Lucifer Yellow within the axoplasm and permeability through the junctional membranes did not remain constant with time but declined. From this it was inferred that Lucifer Yellow experienced a slow, irreversible binding to axoplasmic elements. All three probes had finite plasma membrane permeabilities.

INTRODUCTION

The measurement of solute diffusion through intercellular pathways and cytoplasm is often complicated by cellular size and geometry. Cells are often small and the intercellular junctions occur randomly over the surface of cells. Within a tissue such as liver, diffusion of a solute can occur in three dimensions *in vivo*, or two dimensions in tissue culture. In either case the diffusion of a tracer molecule is determined as an effective or apparent diffusion coefficient. The determinants of the apparent diffusion coefficient are junctional membrane permeability, solute binding to cytosolic and membrane bound proteins, sequestration of the solute into intracellular compartments, tortuosity factors (cytoskeleton and intracellular organelles), and viscosity of the cytoplasm. If the junctional membranes are assumed to occur periodically and perpendicularly to the long axis of a cylindrical tissue bundle (e.g., heart myocardial strips) then junctional permeabilities and apparent cytoplasmic diffusion coefficients can be estimated (Weingart, 1974).

Measurement of cytoplasmic diffusion coefficients of various probes in cells that are true syncytia (e.g., skeletal muscle cells) show a reduction in the diffusion coefficients by a factor of 2 to 100 times relative to those obtained in the aqueous phase (Kushmerick and Podolsky, 1969) or

from the Einstein-Stokes equation. Since the diffusion coefficient of a solute molecule is inversely proportional to solvent viscosity (Einstein-Stokes equation, Robinson and Stokes, 1968) estimates of cytoplasmic viscosity are necessary in determining the other factors that influence the diffusion coefficient of a molecule within a cell. EPR studies in *Myxicola* axoplasm of two low molecular weight spin labels revealed a microviscosity of only 0.02 poise (Rubinson and Baker 1979). Dintenfass (1968) measured the viscosity of erythrocyte cytoplasm at 37°C and found it to be four times greater than water. Cokolet and Meiselman (1969) obtained similar results. More recently, Mastro and Keith (1984) performed electron-spin resonance experiments on cultured cells to assess the rotational and translational motion of solutes within cells. Their studies demonstrate that the viscosity of cytoplasm is greater than the viscosity of water by a factor of 2 to 4 for both motions. Removal of solvent by hypertonic treatment further decreased translational motion by fourfold but suppressed rotational motion only slightly (20% decrease), leading the authors to suggest an increase in the density of cytoplasmic barriers. Greater reductions than those due to viscosity in apparent cytoplasmic diffusion coefficients suggest that some form of solute entrapment occurs within the cytosol, or that there exist cytoplasmic barriers (e.g., tortuosity) to translational motion of solutes.

If intercellular transfer of solutes is mediated by aqueous channels (Bennett, 1977; and Loewenstein, 1975 and 1981), then cytoplasmic diffusion is an important parameter to monitor independent of junctional membrane permeability, to ascertain whether or not solute diffusion is influenced by cytoplasmic factors. These factors could alter the effective concentration gradient of a solute across a junction and therefore the flux of the solute through the junction. Determining whether molecules follow Fickian diffusion reveals information about the transport process in gap junctions and the role of the cytosol in influencing the free pool of solute within the cell.

In the study, the system studied was the septate median giant axon of the earthworm. The septa lie perpendicular to the long axis of the axon (Stough, 1926) and contain gap junctions (Goodenough, 1975; Makowski et al., 1980) or nexuses (Kensler et al., 1979; Gunther, 1975; and Brink and Dewey, 1978), which act as a partial barrier to dye diffusion. This arrangement allows determination of the junctional membrane permeability and the apparent cytoplasmic diffusion coefficient. The intercellular junctions of the septa are typical of those found in invertebrates with the exception of those in the phylum *Arthropoda* (Gilula, 1974; and Brink et al., 1981).

Earlier studies on the earthworm system indicated an inverse relationship between molecular weight and junctional permeability with greatly varying apparent cytoplasmic diffusion coefficients. Only short time intervals could be studied because of the constraints of the model used (Crank, 1975; and Brink and Dewey, 1978 and 1980). The model assumed a single permeant surface with axoplasm on either side extending to infinity. Here we develop a model that allows the determination of junctional membrane permeability (P_j), plasma membrane permeability (P_m) and the apparent axoplasmic diffusion coefficient (D_a) at any time interval for a geometry that is equivalent to that of the septate axon. All three parameters were determined for three fluorescent tracers used extensively in studying intercellular communication. These probes were Lucifer Yellow (LY, $1.26 \times 1.4 \times 0.55$ nm), carboxyfluorescein (CFL, $1.26 \times 1.27 \times 0.85$ nm) and dichlorofluorescein (2CLFL, $1.23 \times 1.27 \times 0.55$ nm). Dimensions were determined from Corey-Pauling (CPK) models.

METHODS

Earthworms (*Lumbricus*) (Carolina Biological Supply Co., Burlington, NC) were maintained in a mixture of soil, leaves, and mulch at 5°C. Nerve cords were dissected as described by Brink and Barr (1977). A trihydroxymethylamine (Tris) buffered saline (pH = 7.4) was used to bath the earthworms during dissection (Prosser, 1973). The dissected cords were transferred to a saline solution that contained 120 mM Na Acetate, 1 mM K Acetate, 1 mM Ca Acetate, 1 mM Mg Acetate, 5 mM Choline Chloride, and 50 μ M Carbachol, pH = 7.5. All experiments were performed in the acetate saline. Individual septate axons were impaled with a microelectrode and one of the three fluorescent probes, LY, CFL, or 2CLFL, was iontophoresed into the cell (Brink and Dewey, 1978). Hyperpolarizing currents of 30 to 80 nA were applied periodically (once every 50 ms) with a duration of 25 to 30 ms for 10 to 30 min to fill cells of

the axon to concentrations of 0.2 to 1 mM. The concentration of a probe inside the axon was estimated by measurement of the fluorescence intensity (Brink, 1983). When the concentration of the fluorescent probe exceeded 2 mM, fluorescence quenching was observed in glass cylinders with inside diameters of 100 μ m.

Fig. 1 shows the general experimental setup used to collect and store diffusion data. A grating monochromator in series with the photomultiplier allowed observation of the peak emission of the fluorescence spectra. A 15×50 μ m slit was placed in the optical path before the grating monochromator and photomultiplier to limit the area of measurement and yield high spatial resolution. The source of excitation for the probes was a xenon lamp with a grating monochromator (Farrand Optical Co., Inc., Valhalla, NY). The excitation was delivered to the axons via epi-illumination. The preparation was mounted on a motorized stage (Carl Zeiss, Inc., Thornwood, NY) that could move the field along the long axis of the axon at a constant velocity. For the experiments done in this study the velocity was 100 μ m/s. The resultant photomultiplier output then revealed the spatial distribution of the probe within the septate axon. Scans were taken at various time intervals and the photomultiplier output was monitored by a microcomputer (IBM-PC; IBM instruments, Inc., Danbury, CT) via an analog-to-digital (A/D) converter (Data Translation, Marlboro, MA). The data was stored on hard disk for subsequent analysis. The amount of dye iontophoresed from experiment to experiment was varied such that the initial concentration of dye was ~ 0.2 – 0.3 mM or ~ 1 mM. The gain of the photomultiplier amplifier was set such that 1 mM = 4 V for each dye. The A/D converter has a voltage window of ± 5 V with a 5 mV sensitivity limit. Therefore the apparatus was capable of sensing concentration, as fluorescence intensity, over three orders of magnitude. The lowest concentration detectable was 1 μ M. In each figure showing raw data, the vertical scale is given in volts.

The theoretical diffusion coefficients for LY, CFL, and 2CLFL in water were calculated from the Einstein-Stokes equation: $D_w = kT / (6\pi\eta r)$, where T = absolute temperature and k is Boltzmann's constant (see Table I). The viscosity of water (η) equals 0.01 poise at room temperature (Jacobs, 1967, or Robinson and Stokes, 1968) and r is chosen as one half the widest dimension of the dye molecule as given by CPK models. For this study the diffusion coefficients predicted from the Einstein-Stokes equation (D_w) will be used as reference diffusion coeffi-

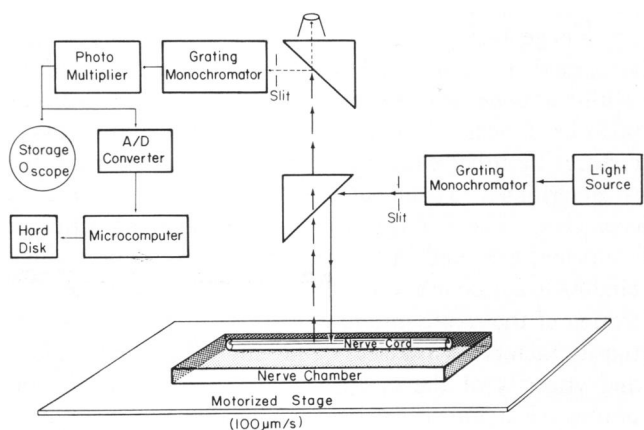


FIGURE 1 Schematic representation of the apparatus used to measure the fluorescence intensity distribution along the long axis of the septate axon is shown. The spatial distribution of the fluorescent probes was monitored by passing the axon, at constant velocity, by a stationary photomultiplier (Brink, 1983). A grating monochromator was used in the excitation path to narrow the spectrum of light delivered to the septate axon via epi-illumination. The grating in front of the photomultiplier further decreased background interference with the fluorescence signal. The area the photomultiplier monitored was 15×50 μ m with a $40\times$ objective.

TABLE I
THEORETICAL DIFFUSION COEFFICIENTS
IN WATER

Dye	D_w	Radius
	cm^2/s	nm
LY	3.1×10^{-6}	0.7
CFL	4.0×10^{-6}	0.635
2CLFL	4.0×10^{-6}	0.635

The radius was taken as half of the widest dimension of the molecule.

cients for assessment of dye behavior in the axoplasm, as has been the convention in other studies (Weingart, 1974; Mastro and Keith, 1984).

THEORY

A schematic representation of the septate axon is depicted in Fig. 2. The individual axons have diameters of $\sim 80 \mu m$, and axon segments can vary in length from 500 to 5,000 μm . We consider an axon filled uniformly at $t = 0$ with a diffusing solute at concentration C_0 . The axon interfaces with two adjacent axons on either side through junctional membranes (P_j). The adjacent cells are assumed to extend to an infinite distance and have no diffusing solute at $t = 0$. In all cells the axoplasmic diffusion coefficient is assumed to be the same and constant in time. Two models for the diffusion of solute in the septate axon will be considered. The first assumes the solute diffuses in the cytoplasm in the longitudinal direction only (one-dimensional model). The second considers both radial and longitudinal transfer of solute (two-dimensional model).

Longitudinal Diffusion with no Plasma Membrane Permeability

The junctional membranes are assumed to be equidistant from $X = 0$ at some distance A (Fig. 2). By virtue of symmetry either of the regions $X \geq 0$ or $X \leq 0$ can be considered. We will consider only $X \geq 0$. The concentrations of fluorescent probe in regions $0 \leq X \leq A$ and $X \geq A$ are denoted C_1 and C_2 , respectively. Let C_0 be the initial concentration of the probe in the injected axon ($0 < X < A$) at time $t = 0$. Let D and P_j denote the diffusion coefficient and the junctional membrane permeability respectively. From Fick's first Law:

$$D(\partial^2 C_1 / \partial X^2) = \partial C_1 / \partial t \quad \text{for } 0 \leq X \leq A \quad (1a)$$

$$D(\partial^2 C_2 / \partial X^2) = \partial C_2 / \partial t \quad \text{for } X \geq A. \quad (1b)$$

By symmetry

$$\partial C_1 / \partial X = 0 \quad (1c)$$

at $X = 0$ for all t

$$D(\partial C_1 / \partial X) = P(C_2 - C_1) \text{ at } X = A. \quad (1d)$$

Conservation demands that

$$\partial C_1 / \partial X = \partial C_2 / \partial X \text{ at } X = A \quad (1e)$$

The boundary conditions are:

$$C_1 = C_0 \text{ for } X \leq A \text{ at } t = 0 \quad (1f)$$

$$C_2 = 0 \text{ for } X \geq A \text{ at } t = 0. \quad (1g)$$

Applying the methods of Laplace transforms where by definition

$$\bar{C}_i = \int_0^\infty \exp(-pt) C_i dt, \quad i = 1, 2$$

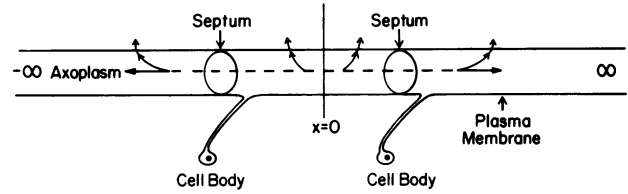


FIGURE 2 Schematic diagram of the axonal model used to analyze the diffusion data. The total area of the septa was assumed to be a permeable surface. Arrows indicate longitudinal diffusion through the axoplasm and junctions (septa) and radial loss across the plasma membrane. The cell bodies are labeled and note that they are small relative to the axon segments. They lie within the neuropile of the nerve cord well away from the axons. Normal injection procedures do not adequately fill the cell body or its process to cause asymmetry in the longitudinal scans of the axons.

and defining $h = P_j/D$ and $q^2 = p/D$, we hypothesize the following relations:

$$\bar{C}_1(X, p) = A_1(p)$$

$$\times \exp(qX) + B_1(p) \times \exp(-qX) + C_0/Dq^2$$

$$\bar{C}_2(X, p) = A_2(p) \times \exp(qX) + B_2(p) \times \exp(-qX),$$

where the barred quantities are the Laplace transform of the corresponding unbarred quantities. Since \bar{C}_2 must approach zero for large X , $A_2(p) = 0$. Solving in the transform-plane for $A_1(p)$ and $B_1(p)$, ($i = 1, 2$), yields:

$$\bar{C}_1(X, p) = C_0/Dq^2 + [C_0 \times h \times \cosh(qX)] / \{Dq^2 \times [q \times \sinh(qA) + h \times \exp(qA)]\} \quad (1h)$$

$$\bar{C}_2(X, p) = -(C_0 \times h/Dq^2) \times [\sinh(qA) \times \exp(-qX + qA)] / (q \times \sinh(qA) + h \times \exp(qA)), \quad (1i)$$

Consideration of the roots of the denominator in the Appendix section 1.1 and subsequent contour integration yields:

$$C_1(X, t) = -2 \times C_0 \times (h^2/\pi) \cdot \int_0^\infty \cos(uX) \times G(u) du \quad \text{for } X \leq A, \quad (1j)$$

and

$$C_2(X, t) = -2 \times C_0 \times (h/\pi) \cdot \int_0^\infty \{u \times \sin(uA) \times \cos[u(X - A)] - h \times \cos(uX)\} \times G(u) du \quad \text{for } X > A, \quad (1k)$$

where u is the integration variable and $G(u)$ is defined by Eq. 11.

$$G(u) = \exp(-Du^2t) \times \sin(uA) / \{u \times [u^2 \times \sin^2(uA) + h^2 - 2 \times u \times h \times \sin(uA) \times \cos(uA)]\}. \quad (11)$$

Longitudinal Diffusion with Finite Plasma Membrane Permeability

The equations for the two-dimensional model are:

$$\partial C_i / \partial t = D[\partial^2 C_i / \partial X^2 + (1/r)(\partial C_i / \partial r) + \partial^2 C_i / \partial r^2] \text{ for } i = 1, 2 \quad (2a)$$

$$\partial C_1 / \partial X = 0 \text{ at } X = 0 \quad (2b)$$

$$D(\partial C_1 / \partial X) = D(\partial C_2 / \partial X) = -P_j(C_1 - C_2) \text{ at } X = A \quad (2c)$$

$$D(\partial C_1 / \partial r) = -P_m \times C_i \text{ for } i = 1, 2 \\ \text{at } r = R; R = \text{axon radius.} \quad (2d)$$

Eqs. 2c and 2d provide the appropriate boundary conditions. Defining Laplace transforms with barred quantities as usual and with $h_m = P_m/D$ we assert the following hypothesis:

$$\bar{C}_1(X, p) = 2 \sum_{n=0}^{\infty} J_0(a_n r) \times \cosh(S_n X) \times A_1(p, a_n) + C_0/Dq^2$$

$$\bar{C}_2(X, p) = \sum_{n=0}^{\infty} J_0(a_n r) \times \exp[(-S_n X) \times B_2(p, a_n)].$$

J_0 and J_1 are the Bessel functions, conventionally defined (e.g., Carslaw and Jaeger, Appendix III, 1959). Substitution into Eqs. 2a to 2d shows that the hypothesis is valid if a_n and S_n satisfy the following equations:

$$a_n \times J_1(a_n R) - h_m \times J_0(a_n R) = 0 \quad (2e)$$

and

$$S_n = (a_n^2 + Dq^2)^{1/2}. \quad (2f)$$

The roots of Eqs. 2e and 2f are given in Carslaw and Jaeger (p.493, 1959).

A_1 and B_2 are then calculated from Eq. 2c:

$$A_1(p, a_n) = -H(a_n) / \\ [2 \times S_n \times \sinh(S_n A) + 2 \times h \times \exp(S_n A)]$$

$$B_2(p, a_n) = H(a_n) \times [\exp(S_n A) \times \sinh(S_n A)] / \\ [S_n \times \sinh(S_n A) + h \times \exp(S_n A)],$$

where

$$H(a_n) = (h \times C_0/Dq^2) \times [2 \times a_n \times J_1(a_n \times R)] / \\ \{R \times (h_m^2 + a_n^2) \times [J_0(a_n R)]^2\}.$$

Evaluation of the roots in Appendix section 1.2 and subsequent contour integration gives Eqs. 2g and 2h.

$$C_1(X, t) = C_0 - 4 \times C_0 \times (B_0/R^2) - 8 \times C_0 \\ \times h^2 \times (B_1/\pi \times R^2) \times \int_0^{\infty} \cos(uX) \times G(u) du \quad (2g)$$

for $X \leq A$

$$C_2(X, t) = 8 \times C_0 \times h \times (B_1/\pi \times R^2) \times \int_0^{\infty} \{u \times \sin(uA) \\ \times \cos[u(X - A)] - h \times \cos(uX)\} \times G(u) du \quad (2h)$$

for $X \geq A$, where

$$B_0 = \sum_{n=0}^{\infty} h_m^2 / [a_n^2(h_m^2 + a_n^2)]$$

and

$$B_1 = \sum_{n=0}^{\infty} \exp(-a_n^2 \times t \times D) \times h_m^2 / [a_n^2(h_m^2 + a_n^2)],$$

and $G(u)$ is once again defined by Eq. 11. Eqs. 2g and 2h are the solutions

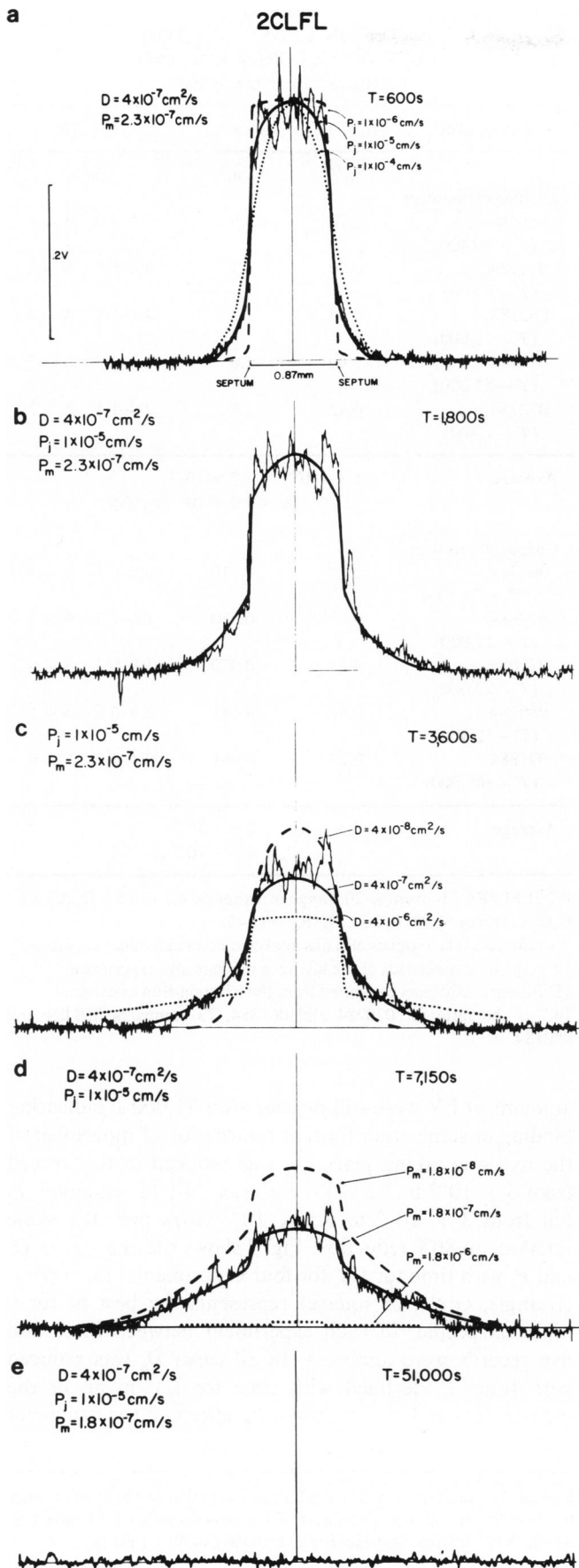
to the two-dimensional equations (Eqs. 2a through 2d) and were used to fit the data for the three fluorescent probes used in this study.

Implementation

All the integrals used in the calculation of concentration were evaluated by the adaptive quadrature method. Accuracy was monitored by checking against the known profiles at the initial time ($t = 0$) to an accuracy of three decimal places for a range of D_a , P_j , and P_m values. Roots of functional Eqs. 2e and 2f were taken from standard tables and linearly interpolated, a technique valid for the ranges of (R/A) used. A typical time for the evaluation of an integral is ~ 15 – 20 s in compiled BASIC for the IBM-PC (IBM Instruments, Inc.)

RESULTS

For the probes 2CLFL and CFL, D_a and P_j remained constant in time, while P_m declined in time. Five individual diffusion profiles of dichlorofluorescein from a single experiment are shown in Fig. 3. In frames *a*, *c*, and *d* of Fig. 3, P_j , D_a , or P_m were varied, respectively, while the other two were held constant, to demonstrate the effect each parameter had on the fitting of the data. In frame 3 *a*, three curves are displayed with the diffusion profile to demonstrate the effect of P_j on the diffusion model profile used to analyze the data. Both D_a and P_m were held constant. The dashed line represents a case where $P_j = 1 \times 10^{-6}$ and the dotted line $P_j = 1 \times 10^{-4}$ cm/s. The solid line represents the case that best fits the data where $P_j = 1 \times 10^{-5}$ cm/s. Fitting was done by eye. The entire surface of the septum was assumed to be accessible by the dye (contact in the plane perpendicular to the long axis of the axons). In Fig. 3 *b* ($t = 1,800$ s), the same parameters that fit the data of 3 *a* were used. In Fig. 3 *c*, D_a was varied while P_j and P_m were held constant. Three values of D_a were used, 4×10^{-8} (dashed line), 4×10^{-7} (solid line), and 4×10^{-6} (dotted line). The best fit for D_a was 4×10^{-7} cm²/s, a value an order of magnitude less than would be predicted from the Einstein-Stokes equation for a 1.2 nm diameter molecule. In frame 3 *d*, P_m was varied over two orders of magnitude. The dashed line represents a P_m of 1.8×10^{-8} and the dotted line a value of 1.8×10^{-6} . The best fit for 3 *d* (solid line, $t = 7,150$ s) was a P_m of 1.8×10^{-7} cm/s. Both P_j and D_a were held constant at 1×10^{-5} and 4×10^{-7} respectively. P_m declined from 2.3×10^{-7} cm/s to 1.8×10^{-7} cm/s between 3,600 s and 7,150 s. In all five experiments analyzed (Table II) for the dye 2CLFL, P_m showed a decline in time while the other two parameters remained constant. In all cases at least three and as many as six records were analyzed from each experiment. The model assumes that all dye that leaks out of the plasma membrane is washed away so that the only decline in the radial concentration gradient comes from the decline of dye concentration in the axoplasm. The reduction of P_m with time suggests that the dye is not washing away to infinite dilution but that significant amounts are present in the periaxonal space and loose myelin covering of the axon. If dye fading with light exposure was a significant contributor to apparent dye loss in the axon, then the model would



predict an increase in plasma membrane permeability with time. This was not found in any of the records analyzed but rather a decline in P_m was observed. Changes in radius of the axon with time will also affect P_m . Therefore the diameter of the injected cells was monitored during the experiments. No diameter changes were observed. In the case of Fig. 3 the axon diameter would have to narrow from 80 to 60 μm . Fig. 3 *e* shows that the dye was no longer detectable by the photomultiplier 51,000 s after injection, and the model predicted that the dye concentration in the axon was $< 0.001\%$ of the original concentration in the injected cell using the fit parameters of 3 *d*. If a large portion of the dye had been bound or trapped in an irreversible fashion within the axon some fluorescence would still be expected to be observed within the axon at the 50,000 s mark.

Five diffusion profiles of the dye carboxyfluorescein are shown from a single experiment in Fig. 4 with the best fit for each spatial distribution. Both D_a and P_j remained constant (Table II) over the time interval studied, but P_m declined 37% over a 17,100 s interval. This decline is presumably due to the accumulation of dye in the periaxonal space as described for 2CLFL. Once again no change in the radius of the axon was observed. Trace amounts of CFL were detectable in axons 150,000 s after injection as the insert in frame 4 *e* shows. The residual fluorescence of CFL indicates a small fraction of dye may irreversibly bind to components of the axoplasm and axolemma or have a very slow dissociation rate with those components.

In Table II the ratios of P_j , D_a , and P_m for 2CLFL and CFL are given. The P_j mean ratio for 2CLFL/CFL was 19.7 with a range of 4.7 to 73, and the D_a ratio was 1.08. The range over which D_a varied for both dyes was 2.8 and the data sets overlapped almost completely. The D_a ratio indicates that 2CLFL and CFL are affected similarly by axoplasmic factors. The P_m ratio followed the same trend as the P_j with a mean ratio of $\sim 5:1$.

Four diffusion profiles of LY from a single experiment are shown in Fig. 5. Unlike the two previous dyes, D_a , P_j , and P_m for LY all declined with time. D_a declined 70%, P_j declined 88%, and P_m was reduced $\sim 50\%$ over a 28,000 s interval. The D_a for LY started out quite high ($2.0 \times 10^{-6} \text{ cm}^2/\text{s}$); a value close to the value expected from diffusion in water. The reduction of D_a with time indicated that the dye was binding or complexing in some form with axoplasmic elements as Stewart (1978) has already suggested. Fig. 6 shows another experiment where significant

FIGURE 3 Fluorometric data for 2CLFL. 3 *a* shows diffusion 600 s after injection of the dye was terminated. The solid smooth line is the best fit by eye for the data. The dashed and dotted lines represent fits where P_j was varied while D_a and P_m were held constant. 3 *b* shows the best fit at 1,800 s. 3 *c* shows the best fit at 3,600 s and the effect of varying D_a . 3 *d* shows the effect of varying P_m . In 3 *e* the data show that no dye is present at 50,000 s and the model predicted a concentration in the injected cell of 0.001% ($4 \text{ V} = 1 \text{ mM}$).

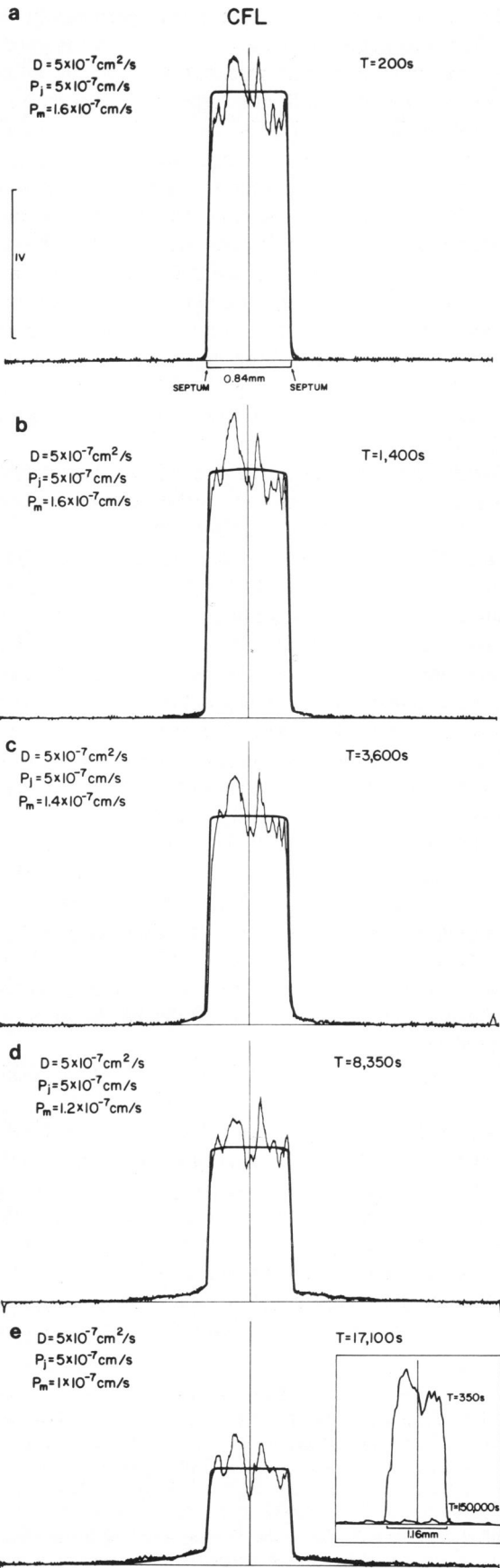


TABLE II
DIFFUSION CONSTANTS FOR
DICHLOROFLUORESCIN AND
CARBOXYFLUORESCIN

Experiment	$D_a \times 10^6$	$P_j \times 10^5$	$P_m \times 10^7$
	<i>cm²/s</i>	<i>cm/s</i>	<i>cm/s</i>
Dichlorofluorescein			
050484 (<i>T</i> = 10,400)	0.70	3.0	5.1–2.0 <i>N</i> = 4
051184 (<i>T</i> = 8,800)	0.80	1.1	4.0–1.8 <i>N</i> = 3
062184 (<i>T</i> = 11,000)	0.35	1.2	4.1–1.9 <i>N</i> = 4
070284 (<i>T</i> = 51,000)	0.40	1.0	2.3–1.8 <i>N</i> = 5
072784 (<i>T</i> = 1,400)	0.42	2.2	2.0–1.4 <i>N</i> = 3
Average	5.3×10^{-7}	1.7×10^{-5}	$D_w = 4.0 \times 10^{-6} \text{ cm}^2/\text{s}\S$
Carboxyfluorescein			
061384 (<i>T</i> ‡ = 20,600)	0.7	0.210	0.2–0.1 <i>N</i> = 6
070684 (<i>T</i> = 17,000)	0.5	0.050	1.6–1.0 <i>N</i> = 5
072084 (<i>T</i> = 23,000)	0.42	0.070	1.0–0.7 <i>N</i> = 4
080184 (<i>T</i> = 12,800)	0.60	0.041	0.9–0.6 <i>N</i> = 5
091884 (<i>T</i> = 105,000)	0.25	0.061	0.4–0.2 <i>N</i> = 6
Average	4.9×10^{-7}	8.6×10^{-7}	$D_w = 4.0 \times 10^{-6} \text{ cm}^2/\text{s}\S$

$P_j/2\text{CLFL}/P_j\text{CFL}$ average 20; range of variation 4.7 to 73. || $D_a/2\text{CLFL}/D_a\text{CFL}$ average 1.08. $P_m/2\text{CLFL}/P_m\text{CFL} \sim 5$.

**N* represents the number of scans analyzed in an individual experiment.

‡*T* is the time in seconds of the last scan made in any experiment.

§Diffusion coefficients computed from the Einstein-Stokes equation.

||4.7 is the ratio for 070284 and 061384, 73 compares 050484 and 080184.

amounts of LY were still present after 71,000 s, indicating binding or some other form of retardation of movement of the dye was taking place. D_a was reduced in this record from 3×10^{-6} to $7 \times 10^{-8} \text{ cm}^2/\text{s}$, a 50-fold reduction. P_j fell from 3×10^{-6} to $6.5 \times 10^{-7} \text{ cm/s}$ over the same interval, an 80% reduction. Fig. 7 shows the changes in D_a and P_j with time for LY for four experiments. Each point (triangle, circle, or square) represents the best fit for a diffusion profile. In each experiment between three and five records were analyzed. In all cases D_a was reduced with time. P_j declined with time for LY in all of the experiments as Fig. 7 *b* shows. P_m mirrored the decline of

FIGURE 4 Analysis CFL in a similar fashion to that of Fig. 3 where only the best fits are shown. The insert of 4 *e* shows another CFL injection which shows residual fluorescence at 150,000 s (4 V = 1 mM).

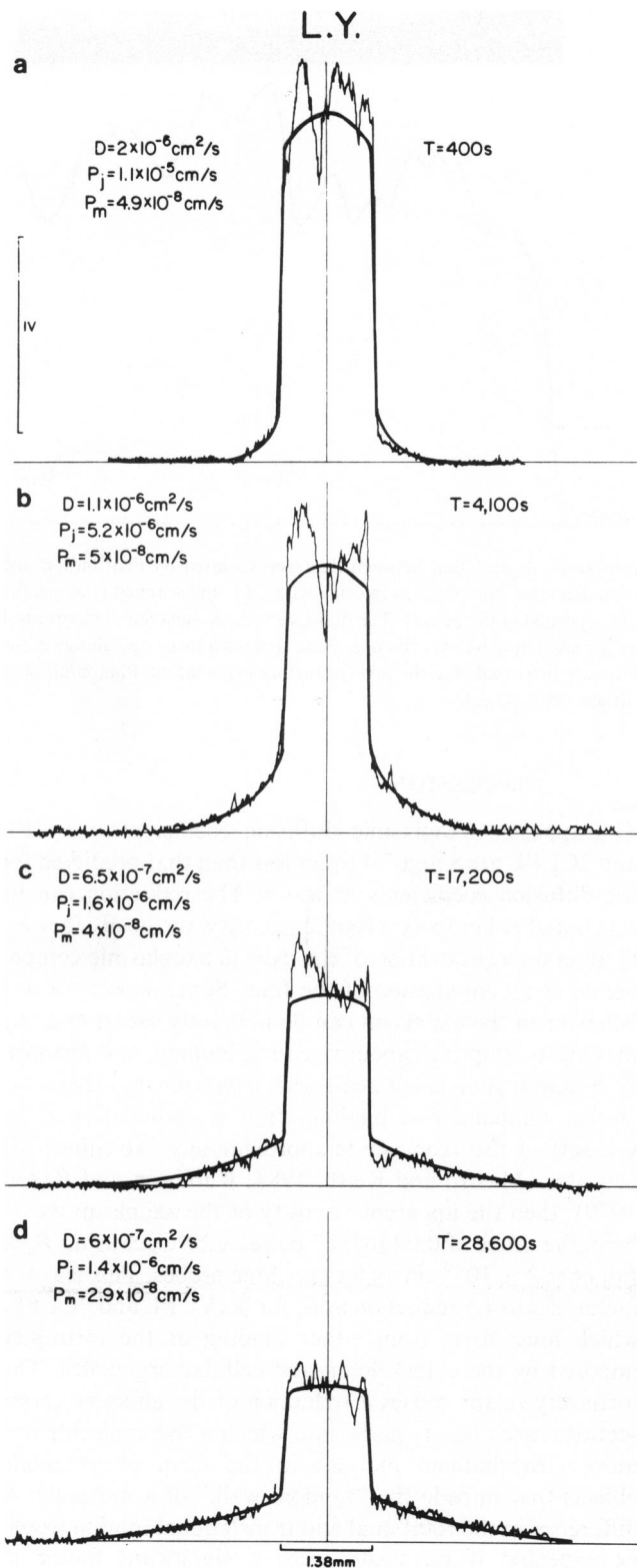


FIGURE 5 Fluorometric data for LY. In all cases, D , P_j , and P_m decreased with increased time after injection. The dye concentration was in the 0.4–0.5 mM range ($4V = 1 \text{ mM}$).

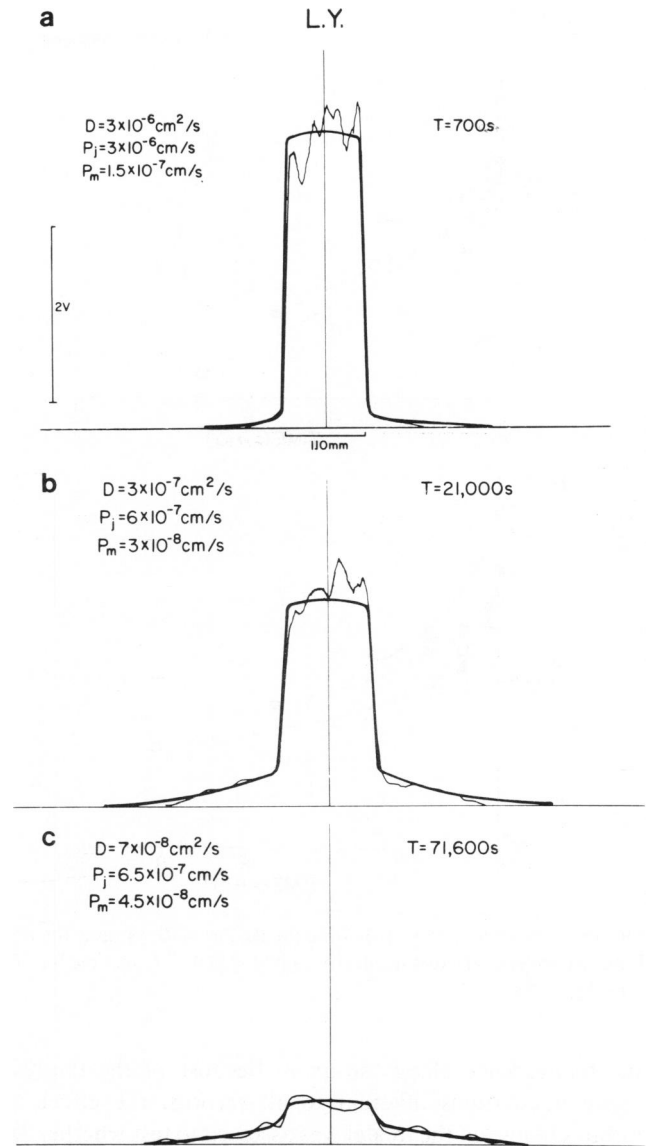


FIGURE 6 The same as Fig. 5 but the initial concentration was 0.9 mM and the diffusion was monitored for a much longer time.

P_j with time. A decline in P_j would be expected if the pool of freely diffusing LY declined due to binding, therefore decreasing the number of molecules that can diffuse through the junction.

In all of the diffusion profiles the fluorescence intensity varied as much as 20–30% within the injected axon where the model predicted smooth curves. Fluctuations of fluorescence intensity along the axon were caused by the fact that the axon diameter varied as much as 50% from one region to the next. Fig. 8 shows a diffusion profile for the dye CFL and a fluorescence micrograph of the same cell. Assuming an even distribution of dye within the axon, those areas of smaller diameter will present less fluorescence intensity to the slit of the photomultiplier than regions of greater diameter, thus producing oscillations in

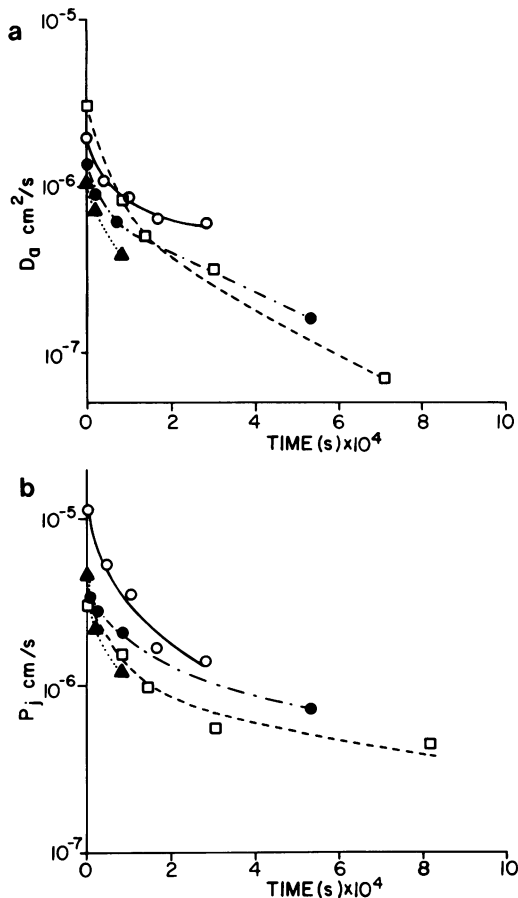


FIGURE 7 (a) Semi-log plot showing the decline of D_a vs. time for LY from four individual experiments. (b) Semi-log plot of P_j vs. time for the same experiments.

the fluorescence along the axon. Because of the fluorescence fluctuations inherent to all records, the effect of radius change on the model was assessed to test whether D_a and P_j were independent of radius. Neither P_j nor D_a were influenced by increasing or decreasing axon diameter while changing P_m proportionately. In all cases P_m had to be altered linearly with changes in diameter to fit the data of Fig. 3 c, indicating that P_m was affected by the surface-to-volume ratio of the cell. Thus P_j and D_a are insensitive to changes in radius. In Figs. 3 and 4 the longitudinal waveform remains relatively constant from scan to scan as Fig. 8 suggests. But in Figs. 5 and 6, which depict LY diffusion, the longitudinal waveform does not remain constant for all times (i.e., peaks and, most notably, valleys appear and disappear). This variation in the LY profiles is most probably related to localized binding (sequestration) to cytosolic and membrane-bound elements. Localized regions either salt out the dye, rendering it nonfluorescent or possibly bind or sequester the dye, decreasing its fluorescence efficiency thus causing a decline in fluorescence intensity. With time, more dye diffuses in from adjacent regions, causing an increase in intensity. Note that CFL and 2CLFL are not affected in this way.

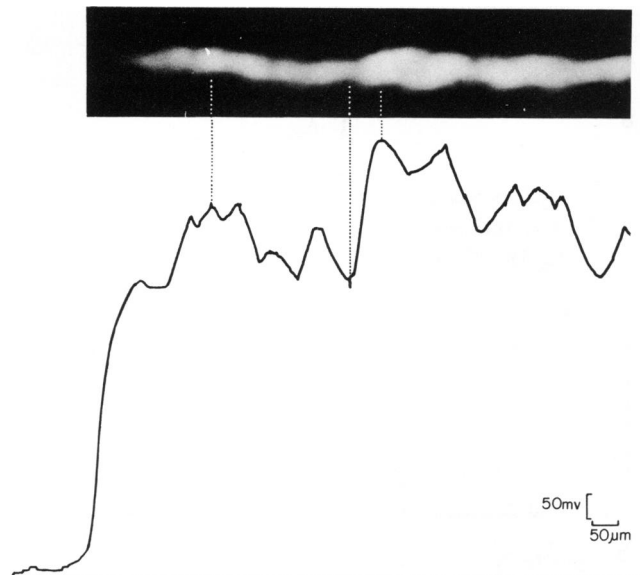


FIGURE 8 Correlation between fluorescence intensity distribution and axon diameter. An axon was injected with CFL and scanned (trace in the lower portion of the figure). The fluorescent axon was then photographed on a Zeiss Universal Microscope. Note that with increased diameter the intensity increased. See the text for further explanation. Photomultiplier slit was $15 \times 50 \mu\text{m}$.

DISCUSSION

The apparent axoplasmic diffusion coefficients for CFL and 2CLFL are 8 and 7.4 times less than that predicted for the diffusion coefficients in water. The reduction can be attributed either to axoplasmic viscosity, tortuosity factors, binding or sequestration of the dyes to axoplasmic components, or a combination of the four. Some aspects of dye behavior in the axoplasm can be indirectly ascertained by making assumptions about viscosity, binding, and tortuosity. Sequestration is not dealt with separately but is considered a component of binding. If it is assumed that the viscosity of the axoplasm is approximately two times that of water (Mastro and Keith, 1984; Rubinson and Baker, 1979), then the apparent viscosity of the axoplasm would be in the range of 0.02 to 0.03 poise at 20°C , causing D_a to fall near $2 \times 10^{-6} \text{ cm}^2/\text{s}$ for the three probes. This leaves a factor of 3 to 4.5 reduction in D_a for both CFL and 2CLFL, which must arise from either binding or the tortuosity imposed by the cytoskeleton and cellular organelles. The tortuosity factor causes a reduction of the effective cross-sectional area in any plane into which a dye molecule can move (translational motion) in the form of immobile objects that impede the "random walk" of a molecule. A difference in the rotational and translational motion would be expected if tortuosity were a significant factor in determining the value of the diffusion coefficient for a molecule. In cultured mammalian cells this was not found to be the case (Mastro and Keith, 1984), thus tortuosity is probably not a significant factor in influencing D_a . If tortuosity were the major factor causing the reduction of

dye diffusion, then cytoskeletal and organelle density would be such that ~60–90% of the cross-sectional area would be occupied by them. The last factor that can cause a reduction in D_a is binding of dye molecules to components of the axoplasm and axolemma. The effects of nonspecific (nonsaturable) reversible binding on diffusion can be assessed using the following:

$$D_a = (M_f/M_t) \times D_f, \quad (3)$$

where M_f is the mole fraction that is free in the axoplasm; M_t is the total molar concentration in the axon such that $M_t = M_f + M_b$; M_b is the mole fraction bound; D_f is the diffusion coefficient for a solute in the axoplasm unimpeded by binding. The diffusion coefficient of the bound solute (M_b) is D_b . This analysis requires that $D_b \ll D_f$ or $D_b \rightarrow 0$. Thus the bound solute is considered to have no translational motion.

For the case of saturable binding, if it is assumed that the reaction is irreversible or that the rate of dissociation is orders of magnitude slower than the rate of association, then Eq. 3.1 can be used to assess the mole fraction bound. Once again D_b must be much smaller than D_f ($D_b \ll D_f$). This assumption does not appear to be unreasonable when the LY data is considered. In the case of LY a significant residual fluorescence remains and can be visualized days after injection.

If D_b approximates D_f then dC/dx will have more than one diffusion profile along the x axis and Eq. 3.1 will not hold. Two illustrations of this are shown in Figs. 9 and 10. Fig. 9 is the case of nonspecific binding where $M_b = M_f$ and D_f (2×10^{-6}) is 10-fold greater than D_b (2×10^{-7}). Note that in the adjacent cells two distinct diffusion profiles can be seen. While the data do not suggest this kind of behavior they cannot unambiguously eliminate this possibility. The diffusion profile of Fig. 10 was generated using the diffusion model. In both cases C_0 was set at 0.5 and the two resultant curves were summed. Fig. 10 illustrates the case

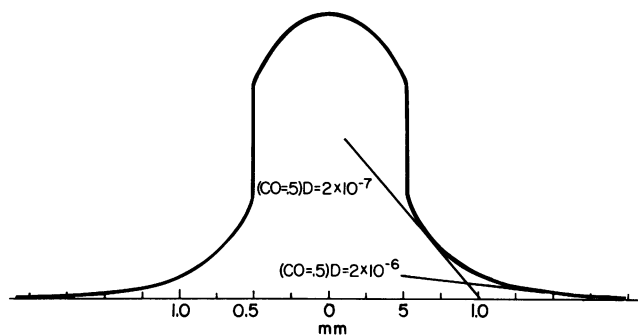


FIGURE 9 Hypothetical diffusion profile where the probe is assumed to be nonspecifically bound to axoplasmic elements. Both P_j (1×10^{-3}) and P_m (1×10^{-7}) were assumed to be the same for the bound and unbound fractions. It was also assumed that at any time the concentration of dye would be equally split between bound and unbound form (50% bound, 50% free). The D_a for the freely diffusing pool was 2×10^{-6} and that of the bound to be 2×10^{-7} cm²/s ($CO = 0.5$). A time of 2,000 s was used.

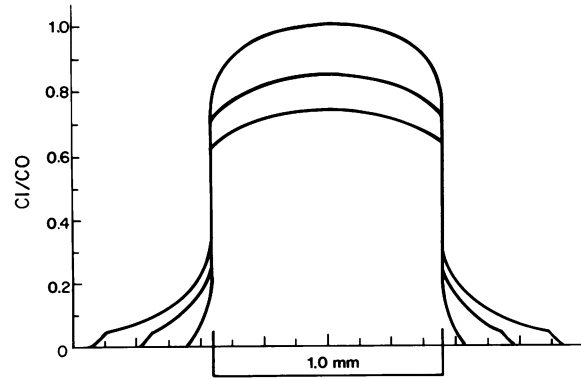


FIGURE 10 Hypothetical diffusion profile where a high affinity binding site is present in the axoplasm. The concentration of the site is 10% of the initial concentration of the monitored tracer. Times were set at 600, 1,000, and 2,000 s. The ratio C_1/C_0 is the ratio of the concentration of the diffusing solute at any x and t vs. the initial concentration of solute at $t = 0$.

where a saturable binding site with a D_b 10-fold less than D_f must first be loaded due to its high affinity for the solute. The concentration of the binding site is one-tenth that of the initial dye concentration. The diffusion profiles in the adjacent cells show first the diffusion profile determined by the slowly diffusing binding sites; then the unimpeded mole fraction begins to dominate the diffusion profile. The diffusion model was used to generate the curves by setting C_0 for the bound solute at 0.1 and C_0 for the freely diffusing solute at 0.9. The diffusion profile of the bound component was plotted as the leading edge of the profile. It was assumed that the association rate is much greater than the dissociation rate. The data did not show this kind of behavior.

If as already stated it is assumed that $D_b \ll D_f$, then Eq. 3 can be used to estimate the amount of bound dye. The fact that both CFL and 2CLFL do not leave significant residual fluorescence in the injected and adjacent cells, and D_a and P_j remain constant for CFL and 2CLFL argues strongly for nonspecific binding of these two molecules. If the viscosity of the axoplasm is assumed to be that of water, then the percent of bound dye for CFL is 88% (Eq. 3) or 76% with a viscosity two times that of water (Mastro and Keith, 1984). For 2CLFL the bound fractions would be 85% or 73%, making the same assumptions about viscosity as were made for CFL. These estimates of bound dye fraction cannot account entirely for the retarded value of D_a relative to water but do demonstrate to a first approximation that nonspecific binding is a major determinant in establishing the free pool for these dyes. In Table III D_a/D_w and percent dye bound are given for all three dyes. The computed D_a for LY at short time intervals is reduced 45% relative to D_w . This reduction is consistent with the notion that at least initially, LY is slowed by cell water viscosity only. With time D_a declines (Fig. 7), indicating that the dye is effectively bound to components of the axoplasm and axolemma; Eq. 3 indicates that the binding is ~95%

TABLE III
COMPARISON OF DIFFUSION COEFFICIENTS IN
AXOPLASM AND WATER

Dye	D_a/D_w	% Bound*
CFL	0.12	76
LY	0.55‡	0
	0.02§	95
2CLFL	0.13	73

*% bound based on an axoplasmic viscosity 2 times that of water.

‡For short time intervals after injection (<1,500 s). P_j and D_a values for LY are taken as the average value from the data of Fig. 7.

§For long time intervals (>20,000 s).

effective. Whether the binding is high affinity or low affinity it appears to be irreversible for LY. The maximum and minimum values of D_a/D_w for LY are shown in Table III, illustrating the decline of D_a with time. The D_a/D_w ratio for the other two molecules remained constant in time.

The ratio of D_a2CLFL/D_aCFL was 1.08 (Table II). This implies, but does not unequivocally mean, that the two dye molecules experience the same impediments to diffusion in the intracellular compartment(s). The ratio of D_aLY/D_a2CLFL or D_aCFL was ~4, using D_a values of LY for short time intervals. This indicates that LY is not being affected by the same axoplasmic components as are CFL and 2CLFL (e.g., nonspecific binding).

Because CFL and 2CLFL have similar values of D_a , a comparison of junctional membrane permeability can be made. CFL has a P_j that is reduced by a factor of 4.7 to 73 relative to that of 2CLFL. Both size and charge play an important role as determinants of solute mobility within the junctional channels (Loewenstein, 1981; and Brink and Dewey, 1980). CFL has dimensions of $1.26 \times 1.27 \times 0.85$ nm and has two carboxyl groups with pKs in the range of 3–4. 2CLFL has dimensions of $1.23 \times 1.27 \times 0.55$ nm with only one carboxyl group. The only size difference is the narrowest dimension. If the channel is assumed to have a more or less spherical orifice with its narrowest dimension being ~1.5 nm (Makowski et al., 1984; and Loewenstein, 1981), then the limiting dimensions for CFL and 2CLFL are 1.26 and 1.23 nm respectively. The lack of dimensional disparity strongly suggests a role for charge not only on the solute but also within the junctional channel in determining the permeability of the junctional membrane. These results are consistent with the concept of fixed charge groups within or at the entrance of the intercellular channel (Brink and Dewey, 1980 and Flagg-Newton et al., 1979) which in effect, by virtue of field effects, present channel diameters of different sizes to solutes depending on the surface charge density of the solute molecule diffusing through the junctional channel.

Experiments using heavy water exchange show an activation energy difference between D_2O saline and H_2O of 0.8–1.0 kcal/mol for both dye diffusion (Brink, 1983) and conductance (Brink et al., 1984) indicating that there is

some form of hydrogen or deuterium bonding between solute and channel. The earthworm septal junctions do not show transjunctional voltage-sensitive conductances as do amphibian and teleost blastomeres (Spray et al., 1981 and 1984) but do show pH sensitive conductances (Verselis and Brink, 1984). In the earthworm the pH sensitivity is of questionable physiological significance but does imply that titratable charge groups near or within the channel are present. These proposed charge groups and/or gates could be responsible via field effects for the reduced P_j of CFL relative to 2CLFL.

The binding of the dyes to the axoplasm reduces the effective free concentration of the dye in the cell, and since the model assumes all the injected dye is free to diffuse, the computed values of P_j are suppressed. Correcting for the binding (Eq. 3) elevates P_j ~ eightfold for CFL and 2CLFL. Thus P_j would be $\sim 1 \times 10^{-4}$ cm/s for 2CLFL and 6×10^{-6} cm/s for CFL. No such correction need be made for LY since, at least initially, the dye appears to diffuse in the axoplasm with viscosity as the major determinant of D_a .

In conclusion, the dyes LY, CFL and 2CLFL were shown to diffuse nonideally in the axoplasm of the septate axon. In the case of CFL and 2CLFL D_a was reduced by a factor of 8 while LY behavior was indicative of a slow binding process or sequestration. Note that LY in K^+ salt solutions precipitates as a K salt and is nonfluorescent in that form. But inside cells it is quite fluorescent and at least in the earthworm appears to be nontoxic even with exposure to light (Brink et al., 1984). The slow decline in D_a , P_j , and P_m may be an indication of a slow salting out of dye with K^+ . Finally the data suggests that both size and charge are important in determining the diffusion rate of a molecule in the intercellular channel and that, to fully understand the rate of transfer across the junction of a solute molecule, the behavior of the solute within the cytosol of the cell must be assessed. Diffusion modeling of the sort utilized in this study also has potential significance in the modeling of embryonic systems where morphogens are thought to play a significant role in cellular differentiation.

APPENDIX

Section 1.1

For the purposes of contour integration we need to know if C_1 and C_2 are multivalued. The roots of the denominator of C_1 and C_2 in the complex p -plane must also be evaluated. Fortunately, both C_1 and C_2 share the same denominator, which is:

$$Dq^2[q \times \sin h(qA) + h \times \exp(qA)] \text{ where } q = \sqrt{p/D}. \quad (A1)$$

The square root of p defines the denominator as multivalued. To make it single valued we define a branch cut in the complex p -plane extending from $p = 0$ to $p = -\infty$ along the real axis. The roots of the denominator are evaluated as follows: One obvious root is $p = Dq^2 = 0$. The possible roots of $[q \times \sin hqA + h \times \exp(qA)]$ must also be considered. If q is purely imaginary such that $q = i\eta$ then Eq. A1 gives $\exp(2 \times i\eta \times A) = i\eta/(i\eta + 2h)$. This yields the modulus $\eta^2 = \eta^2 + 4h^2$, which excludes

imaginary roots. It can also be shown that q cannot be a complex root of the form $(\epsilon + i\eta)$ by the standard method (Carslaw and Jaeger 1959, p. 325). For this consider the function U , defined as follows:

$$U_1 = \exp(-bA) \times \cosh(bX) \text{ for } 0 < X < A$$

$$U_2 = -(1/h) \times [h \times \cosh(bA) + b \times \sinh(bA)]$$

$$\times \exp(-bX) \text{ for } X > A,$$

where b satisfies Eq. A2:

$$b \times \sinh(bA) + h \times \exp(bA) = 0. \quad (\text{A2})$$

Then it can be shown that: $d^2U_i/dX^2 - b^2U_i = 0$ where $i = 1, 2$; $dU_1/dX = 0$ for $X = 0$; $U_2 = 0$ as X approaches infinity; $dU_1/dX = b \times \exp(-bA) \times \sinh(bA)$ at $X = A$, and thus $dU_1/dX = -h(U_1 - U_2)$ at $X = A$; $dU_1/dX = dU_2/dX$ at $X = A$. Let b and a be two different roots of Eq. A2 and U_i and V_i be the corresponding quantities. Then it can be proved (Carslaw and Jaeger, 1959) that:

$$(b^2 - a^2) \left[\int_0^a (U_1 \times V_1) dX + \int_a^\infty (U_2 \times V_2) dX \right] = 0. \quad (\text{A3})$$

If a and b are complex conjugates of the form $\epsilon \pm i\eta$ then $(b^2 - a^2)$ cannot equal zero but since U_1, V_1 , and U_2, V_2 are complex pairs, the term in square brackets is positive (Eq. A3) and there is a contradiction. Thus all roots of $h \times \exp(bA) + b \times \sinh(bA)$ are real. But since $b \times \sinh(bA) > 0$ for all b and $h \times \exp(bA) > 0$ for all real b , we conclude that $h \times \exp(bA) + b \times \sinh(bA)$ has no roots at all, thus allowing us to invoke the inversion theorem. The contour of integration is chosen to avoid the pole at $p = 0$, and the branch cut along the negative real axis. Contour integration then yields Eqs. 1h and 1i.

Section 1.2

As in the Appendix, section 1.1, it can be shown the denominator $[S_n \times \sinh(S_n A) + h \times \exp(S_n A)]$ does not have any roots at all (Carslaw and Jaeger, 1959). It is also necessary to determine if A_1 and B_2 are multivalued. There is a root due to $p = Dq^2$ at $p = 0$ and C_1 and C_2 both involve $S_n = (Dq^2 + a_n^2)^{1/2}$ and are hence multivalued functions. To make them single valued we define a branch cut from the root of $S_n = 0$, therefore from $Dq^2 = p = -a_n^2$ to $-\infty$ along the real axis. The contour of integration is now chosen to avoid the pole at $p = 0$ and the branch cut from $-a_n^2$ to $-\infty$ along the negative real axis.

The authors would like to thank Drs. Jaslove and Kasianowicz for their helpful and careful discussions.

This work was supported by National Institutes of Health grant GM 29405 and National Science Foundation grant 83-14295.

Received for publication 26 December 1984 and in final form 8 April 1985.

REFERENCES

- Asada, Y., and M. V. L. Bennett. 1971. Experimental alteration of coupling resistance at an electrotonic synapse. *J. Cell Biol.* 49:159-172.
- Bennett, M. V. L. 1977. Electrical transmission: A functional analysis and comparison to chemical transmission. In *The Handbook of Physiology*. Sec. 1. The Nervous System. E. Kandel, editor. American Physiological Society, Washington. 357-416.
- Brink, P. R. 1983. Effect of deuterium oxide on junctional membrane channel permeability. *J. Membr. Biol.* 71:79-87.
- Brink, P. R., and L. Barr. 1977. The resistance of the septum of the median giant axon of earthworm. *J. Gen. Physiol.* 69:517-536.
- Brink, P. R., and M. M. Dewey. 1978. Nexal membrane permeability to anions. *J. Gen. Physiol.* 72:69-78.
- Brink, P. R., and M. M. Dewey. 1980. Evidence for fixed charge in the nexal. *Nature (Lond.)* 285:101-102.
- Brink, P. R., M. M. Dewey, D. E. Colflesh, and R. W. Kensler. 1981. Polymorphic nexuses in the earthworm *Lumbricus terrestris*. *J. Ultrastr. Res.* 77:233-244.
- Brink, P. R., V. Verselis, and L. Barr. 1984. Solvent-solute interactions within the nexal membrane. *Biophys. J.* 45:121-124.
- Carslaw, H. S., and J. C. Jaeger. 1959. *Conduction of Heat in Solids*. 2nd ed. Oxford University Press, Oxford. 505 pp.
- Cokelet, G. R., and H. J. Meiselman. 1968. Rheological comparison of hemoglobin solutions and erythrocyte suspensions. *Science (Wash. DC)* 162:275-277.
- Crank, J. 1975. *The Mathematics of Diffusion*. 2nd ed. Oxford University Press, London. pp. 15, 40.
- Dintenfass, L. 1968. Internal viscosity of the red cell and a blood viscosity equation. *Nature (Lond.)* 219:956-958.
- Flagg-Newton, J., I. Simpson, and W. R. Loewenstein. 1979. Permeability of cell-to-cell membrane channels in mammalian cell junctions. *Science (Wash. DC)* 205:4404.
- Gilula, N. Junctions between cells. In *Cell Communication*. R. P. Cox, editor. John Wiley & Sons, Inc., New York.
- Goodenough, D. 1975. The structure and permeability of isolated hepatocyte gap junctions. *Cold Spring Harbor Symp. Quant. Biol.* 40:37-44.
- Gunther, J. 1975. Neuronal syncytia in the giant fibers of earthworm. *J. Neurocytol.* 4:55-62.
- Jacobs, M. H. 1967. *Diffusion Processes*. Springer-Verlag, Berlin. 160 pp.
- Kensler, R. W., P. Brink, and M. M. Dewey. 1979. The septum of the lateral axon of the earthworm: a thin section and freeze fracture study. *J. Neurocytol.* 8:565-590.
- Kushmerick, M. J., and R. J. Podolsky. 1969. Ionic mobility in muscle cells. *Science (Wash. DC)* 166:1297-1298.
- Mastro, A. M., and A. D. Keith. 1984. Diffusion in the aqueous compartment. *J. Cell Biol.* 99 (1, Pt. 2):180s-187s.
- Makowski, L., D. L. D. Casper, W. C. Phillips, T. S. Baker, and D. A. Goodenough. 1984. Gap junction structures. VI. Variation and conservation in connexon conformation and packing. *Biophys. J.* 45:208-218.
- Loewenstein, W. R. 1975. Permeable junctions. *Cold Spring Harbor Symp. Quant. Biol.* 40:49-63.
- Loewenstein, W. R. 1981. Junctional intercellular communication: the cell-to-cell membrane channel. *Physiol. Rev.* 61:829-913.
- Prosser, C. L. 1973. *Comparative Animal Physiology*. W. B. Saunders Company, Philadelphia. 966 pp.
- Robinson, R. A., and R. H. Stokes. 1968. *Electrolyte Solutions*. Butterworth & Co., Ltd., London. 571 pp.
- Rubinson, K. A., and P. F. Baker. 1979. The flow properties of axoplasm in a defined chemical environment: influence of anions and calcium. *Proc. R. Soc. Lond. B. Biol. Sci.* 205:323-345.
- Spray, D. C., A. L. Harris, M. V. L. Bennett. 1981. Equilibrium properties of a voltage-dependent junction conductance. *J. Gen. Physiol.* 77:77-94.
- Spray, D. C., R. L. White, A. Campos De Carvalho, A. L. Harris, and M. V. L. Bennett. 1984. Gating in gap junction channels. *Biophys. J.* 45:219-230.
- Stewart, W. 1978. Functional connection between cells as revealed by dye coupling with a highly fluorescent naphthalimide tracer. *Cell.* 14:141-159.
- Stough, H. B. 1926. Giant fibers of the earthworm. *J. Comp. Neurol.* 40:409-463.
- Verselis, V., and P. R. Brink. 1984. Voltage clamp of the earthworm septum. *Biophys. J.* 45:147-150.
- Weingart, R. 1974. The permeability of tetraethylammonium ions of the surface membrane and the intercalated disks of sheep and calf myocardium. *J. Physiol.* 240:741-762.